Membranes

International Edition: DOI: 10.1002/anie.201503782
German Edition: DOI: 10.1002/ange.201503782

Growth of High-Quality, Thickness-Reduced Zeolite Membranes towards N_2/CH_4 Separation Using High-Aspect-Ratio Seeds

Yi Huang, Lei Wang, Zhuonan Song, Shiguang Li, and Miao Yu**

Abstract: *Greatly improved zeolite membranes were prepared by using high-aspect-ratio zeolite seeds. Slice-shaped seeds with a high aspect ratio (AR) facilitated growth of thinner continuous SAPO-34 membranes of much higher quality. These membranes showed N_2 permeances as high as $(2.87 \pm 0.15) \times 10^{-7}$ mol m^{-2} s^{-1} Pa^{-1} at 22 °C while maintaining a decent N_2/CH_4 selectivity (9–11.2 for equimolar mixture). On the basis of these thinner high-quality SAPO-34 membranes, fine-tuning the local crystal structure by incorporating more silicon further increased the N_2 permeance by 1.4 times without sacrificing the N_2/CH_4 selectivity. We expect that application of large AR zeolite seeds might be a viable strategy to grow thin high-quality zeolite membranes. In addition, fine-tuning of the crystal structure by changing the crystal composition might be a feasible way for further improving the separating performance of high-quality zeolite membranes.*

According to U.S. natural gas pipeline specifications, inert gases, such as N_2, should be less than 4 %.[1] Currently, N_2 is typically separated by energy-intensive cryogenic distillation (CD) process. Membrane separation technology is a more energy-efficient alternative for N_2 extraction from natural gas.[2] However, applying it for N_2/CH_4 separation is challenging because the kinetic diameter difference between N_2 (0.364 nm) and CH_4 (0.38 nm) is less than 0.02 nm and both molecules are classified as weak adsorbates.[3] The state-of-the-art N_2-selective polymeric membranes, assuming 100 nm membrane thickness, typically exhibit a low N_2 permeance of less than or equal to or 20 GPU (1 GPU = 3.348×10^{-10} mol m^{-2} s^{-1} Pa^{-1}) at N_2/CH_4 selectivities of 3–5, according to "Robeson" plot.[4]

Zeolites are considered as an excellent membrane material because of their molecular-sized pores and high thermal, mechanical and chemical stabilities. Growth of thin zeolite membranes with high-quality/negligible defects is highly desirable yet very challenging by hydrothermal synthesis. Up to now, several zeolite membranes with framework type of MFI,[5] Y,[6] T,[7] DDR,[8] SSZ-13,[3] and SAPO-34[3,9] have been reported to separate CO_2 from CO_2/CH_4 mixtures. However, when applied for N_2/CH_4 separation, they suffer from the low N_2 permeance and/or low N_2/CH_4 separation selectivity. For example, SSZ-13 and SAPO-34 membranes were prepared and investigated for N_2/CH_4 mixture separation in a recent study. SSZ-13 membrane displayed superior N_2/CH_4 separation selectivity of about 13 but with a low N_2 permeance of 2.2×10^{-8} mol m^{-2} s^{-1} Pa^{-1} at 20 °C.[3] SAPO-34 membranes, which have the CHA structure and pore entrance size similar to the kinetic diameter of CH_4, exhibited much higher N_2 permeance of about 1×10^{-7} mol m^{-2} s^{-1} Pa^{-1}. The reported N_2/CH_4 selectivities, however, were between 5 and 8. Considering higher N_2 permeance and favorable crystal pore size, SAPO-34 membranes seem to be a good candidate for N_2/CH_4 separation, although their quality still needs to be drastically improved to increase separation selectivity. Moreover, most of the studied SAPO-34 membranes were thick (typically >5 μm), suggesting great potential for further increase of N_2 permeance.

Layered zeolitic materials in nanosheet form have been used for preparing ultrathin zeolite membranes by combining filtration deposition of a thin zeolite coating with subsequent short period hydrothermal growth. For instance, MFI zeolite nanosheets (ca. 3 nm in thickness) has been applied to the growth of thin MFI zeolite films which showed superior performance in *p*-xylene/o-xylene separation.[10] Although it is highly desirable to use thin zeolite nanosheets for growing zeolite membranes, only MWW and MFI zeolites were currently available in crystalline nanosheet form. Attempts to exfoliate other layered zeolites, including certain layered silicates and aluminophosphates with microporous layers, did not preserve the crystallographic order of the layers.[11] Thus, preparation of zeolite nanosheets or high-aspect-ratio slice-shaped zeolites is still highly challenging, but yet, desirable, for preparing thin and high-quality zeolite membranes.

Towards high N_2 permeance and improving N_2/CH_4 selectivity, we prepared slice-shaped SAPO-34 zeolite seeds and used these seeds with high AR for preparing high-quality thin SAPO-34 membranes. SAPO-34 seeds with larger ARs facilitated the formation of thinner continuous membranes upon secondary crystallization. The exceptional separation performance for equimolar N_2/CH_4 mixture (50/50) was achieved with the thinnest membranes (ca. 2 μm) prepared using seeds with an average AR of 10. To our knowledge, shaped zeolite crystals have shown significant effect on the growth of high-performance membranes.[5c] However, the AR effect of the SAPO-34 seeds on the membrane thickness and its gas separation performance have not been reported before.

[*] Y. Huang, L. Wang, Z. Song, M. Yu
Department of Chemical Engineering
University of South Carolina, Columbia, SC 29208 (USA)
and
SmartState Center of Catalysis for Renewable Fuels
University of South Carolina, Columbia, SC 29208 (USA)
E-mail: yumiao@cec.sc.edu
S. Li
Gas Technology Institute
1700 S. Mount Prospect Road, Des Plaines, IL 60018 (USA)
E-mail: Shiguang.Li@gastechnology.org

Supporting information for this article is available on the WWW under http://dx.doi.org/10.1002/anie.201503782.

Single, dual, and ternary structure-directing agent (SDA) systems have been applied for the synthesis of SAPO-34 crystals.[9a,12] In these systems, tetraethylammonium hydroxide (TEAOH) was normally used as the main SDA to direct SAPO-34 crystallization. It is also beneficial to SAPO-34 growth by adding small amines such as dipropylamine (DPA) and cyclohexylamine as co-SDAs because they can increase crystallization rates and enhance the stabilization and crystallinity of the final products. Carreon et al. used a ternary SDA system (TEAOH, DPA, and CHA) for the synthesis of SAPO-34 seed and a dual SDA system (TEAOH and DPA) for subsequent secondary growth of continuous membranes.[9a] The obtained membranes showed higher fluxes and high selectivities in CO_2/CH_4 and CO_2/H_2 mixtures separation. In this study, the dual SDA system was kept for membrane synthesis to achieve high gas permeation. However, for the seed syntheses, only TEAOH was included. The single TEAOH system eliminated additional effects from secondary SDAs on crystal growth and provided a more straightforward platform to examine the factors that govern the AR of seeds. The concept for growth of thin SAPO-34 crystals with a high aspect ratio was to develop a very reactive system with a high P content (P/(Al + Si + P)) and also with supersaturated Al and Si species. Precursors with high concentration of phosphorous acid have shown their potential to crystallize thickness-reduced SAPO-34 crystals under microwave heating.[2,9] However, an impure phase, such as AEI, might crystallize to form a hybrid AEI-CHA composite. Our study based on hydrothermal crystallization implied that in order to synthesize pure thin SAPO-34 crystals, it was necessary to adjust the synthesis conditions (e.g., aging time and crystallization temperature) to control the rate of crystallization and phase transformation (see Materials and Methods in the Supporting Information). However, the high AR seed growth mechanism is not the focus of this study and will be discussed in details in another study.

In this study, highly crystalline SAPO-34 seeds with average AR of about 1, 3, 10, and 20 and submicron lateral sizes were synthesized hydrothermally (Figure 1) through careful and extensive recipe constructions and fine-tuning of synthesis conditions. The details of synthesis procedure are given in the Supporting Information. XRD patterns of all as-synthesized seeds can be easily indexed to the characteristic CHA structure, indicating that they were phase pure and highly crystalline (Figure 1, XRD).

SAPO-34 cubes with AR of about 1 (denoted as S1, Figure 1a) and particle size distribution in the range of 0.5–1.2 μm (average size = 0.8 μm) were prepared at 200 °C for 24 h using a gel composition of $1.0\,Al_2O_3$:$0.6\,SiO_2$:$1.0\,P_2O_5$:$60.0\,H_2O$:2.0 TEAOH. Thinner seeds with AR of about 3 (denoted as S2, Figure 1b) and 10 (denoted as S3, Figure 1c) were prepared by using a modified gel composition ($1.0\,Al_2O_3$:$0.6\,SiO_2$:$2.0\,P_2O_5$:$75.0\,H_2O$: 4.0 TEAOH) and crystallization at 200 °C and 210 °C, respectively, for 24 h. S2 seeds with a thickness of 0.3 ± 0.075 μm had a fairly uniform lateral size (0.85 ± 0.2 μm), whereas much thinner S3 seeds had a broader lateral size distribution (0.4–1.2 μm). This may be because of the shorter aging time of the gel mixture (72 h) for S3 than that for S2 (144 h). In zeolite synthesis, extended aging of gel mixture favors the formation of more nuclei and thus might affect the size, morphology, and uniformity of the final product. However, the majority of S3 seeds were over 0.6 μm in lateral size and less than 0.1 μm in thickness (Figure S1a,b), which yielded an average AR of 10 (based on size examinations of more than 5000 seeds). It is also worthwhile mentioning that in this sample the AR could reach as high as 20 for a small fraction (6–9 %) of crystals with a thickness of 0.05 μm and lateral sizes over 1 μm (Figure S1c). Moreover, the as-synthesized S3 seeds were highly dispersible in water and easily deposited as oriented layers on flat surfaces, indicative of their good structural stability in thin slice form (Figure S1a).

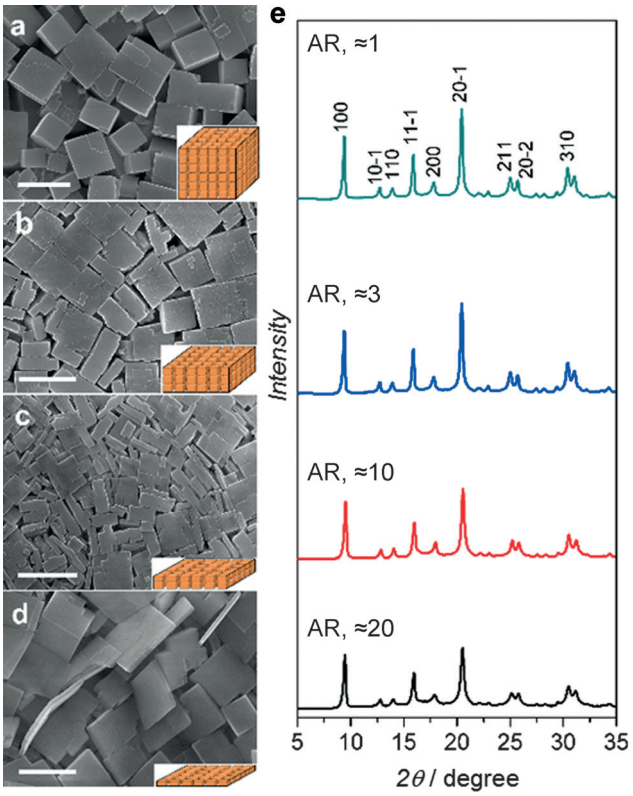

Figure 1. a–d) SEM images and e) XRD patterns of SAPO-34 seeds with average AR of a) 1, b) 3, c) 10, and d) 20. The insets of each SEM images provided a schematic drawing of the typical morphology of a seed. Scale bars in (a), (b), and (c) 1 μm and in (d) 0.5 μm.

SAPO-34 seeds with further reduced thickness (denoted as S4) were also synthesized at 170 °C for 24 h with a gel composition of $1.0\,Al_2O_3$:$0.6\,SiO_2$:$1.0\,P_2O_5$:$55.0\,H_2O$:1.5 TEAOH. Their lateral sizes were in the range of 0.1–0.7 μm (0.5 μm in average) and smaller than those of S1–S3. However, most of the seeds were thinner than 0.05 μm with an average AR of 20 (Figure S2). Some SAPO-34 crystals (ca. 1–3 % in quantity) observed under microscope were as thin as 0.015 μm (15 nm) which corresponds to approximately 10 CHA unit cells (unit cell dimensions: $a = 13.68$ Å, $b = 13.68$ Å, and $c = 14.77$ Å; Figure S2a).[13] Moreover, those thin seeds looked semi-transparent under the scanning electron microscope (SEM) observation with an acceleration voltage of 15 kV, again indicating very thin thickness of the

seeds. More importantly, these very thin SAPO-34 seeds still preserved high crystallinity according to XRD study (Figure 1). To our knowledge, S4 contains the thinnest SAPO-34 crystals reported thus far which corresponds to 10 unit cells in thickness.

To understand the effect of seed AR on membrane growth, SAPO-34 membranes were synthesized by secondary growth on porous tubular α-Al_2O_3 supports with 100 nm pores (Inopor Micro, 100 nm). SAPO-34 seeds in Figure 1 were used to provide nucleation for membrane growth. Note, SAPO-34 seeds were only deposited on the inside surface of the tubular support via a rubbing process (see the Supporting Information for the details of the rubbing process and also procedures of secondary membrane growth). For each seed, 6–9 membranes were prepared at 210 °C for 6.5 h using the same gel, $1.0\,Al_2O_3$:$1.0\,P_2O_5$:$0.3\,SiO_2$:1.0 TEAOH:1.6 DPA:$75\,H_2O$. Mn (n = 1–4) corresponded to batch number of membranes prepared using seeds S1–S4, respectively, while other synthetic parameters were kept the same. All as-synthesized membranes were soaked in deionized water for about 18 h before template removal by calcination, following a previous study.[9d] After that, N_2/CH_4 separation tests (i.e., single and mixture gas tests) were performed for all membranes, while 1–2 membranes in each batch were crashed for characterizations.

The average membrane thicknesses were 6.6 ± 0.3, 4.5 ± 0.4, 2.4 ± 0.25, and 1.8 ± 0.35 μm when using S1–S4 seeds, respectively, as indicated by many SEM images; Figure S3 showed some representative images. As shown in Figure 2 a, the membrane thicknesses decreased monotonically (almost linearly) with increase of the logarithm of the average seed ARs, indicating that the higher-aspect-ratio seeds allowed the formation of thinner membranes. Propane with a kinetic diameter of 0.43 nm has big difficulties in penetrating into SAPO-34 pores. Therefore, its permeation test can be used to identify the flow through defects larger than 0.50 nm.[3]

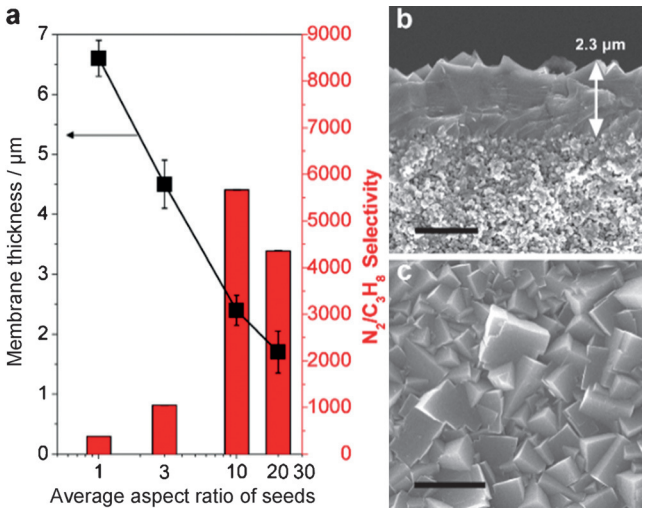

Figure 2. a) Effect of the seed AR on membrane thickness (solid squares) and the N_2/C_3H_8 ideal selectivity (red bars) for corresponding membranes. b) Cross-sectional and c) top-view SEM images of a representative SAPO-34 membrane prepared using S3 seeds. Scale bars in (b) and (c) 2 μm.

Single-gas permeation was measured for N_2 and propane on SAPO-34 membranes (Figure 2 a and Table S1). Interestingly, the thickest M1 (6.5 μm) displayed the lowest N_2/C_3H_8 ideal selectivity of 379 ± 53. The number increased to 1046 ± 120 for M2 (4.6 μm) followed by a dramatic rise to 5665 ± 523 for thinner M3 (2.3 μm). Apparently, the seed AR not only affected the thickness of membranes but also played a crucial role on the control of defect formation. High-aspect-ratio crystals may pack much better, as shown in Figure S1, and form a much thinner seeding layer than cubic crystals. These may help minimize the amount of non-zeolite pores/defects while maintaining a thin membrane thickness. Figure 2 a and b presented top-view and cross-sectional SEM images of a membrane prepared using S3 seeds. SAPO-34 crystals with grain size of approximately 2 μm were well intergrown to form a 2.3 μm thick continuous membrane free of visible defects (e.g., cracks and pinholes; Figure S4a,b).

SAPO-34 membranes prepared with S4 seeds (AR: 20) displayed slightly lower N_2/C_3H_8 selectivity of 4355 ± 205. The effective membrane thickness (Figure S3e) was actually much thicker than the top layer thickness (1.8 ± 0.35 μm) observed under SEM. Partial seed inclusion in the support pores (0.1 μm) may happen during rubbing process. Note, according to SEM observation, S4 contained 5 % of seeds smaller than 0.1 μm in lateral size. Seed inclusion could lead to the formation of thicker membranes with degraded separation performance. Similar results were also obtained by other researchers in attempts to use small seeds.[9c] We expect thinner membranes with improved selectivity would be obtained if supports with smaller pores were used to avoid seed inclusion in support pores. The effect of support pore size and open porosity on the secondary growth of N_2/CH_4 separation SAPO-34 membranes was systematically studied in our recent work.[2]

These membranes were tested for separation of equimolar N_2/CH_4 mixture at 22 °C and a fixed feed and permeate pressure of 275 and 101 kPa, respectively. Separation performance of representative membranes was presented in Table 1. Usually, thicker zeolite membranes were prepared to minimize flux contribution of nonselective defects (non-zeolite pores). This typically leads to increased selectivity and decreased permeance. However, we found an inversed relationship between N_2 permeance and N_2/CH_4 selectivity for the membranes M1–M3, and achieved a simultaneous increase in permeance and selectivity by using seeds with increased ARs (Table 1 and Figure S5). Specifically, N_2 flux

Table 1: CH_4 Separation Properties of SAPO-34 Membranes at 22 °C, a permeate pressure of 101 KPa, and pressure drop of 175 KPa.

Membrane ID	Average AR of Seeds	Permeance [$\times 10^7$ mol m^{-2} s^{-1} Pa^{-1}]		N_2/CH_4 Mixture Selectivity
		N_2	CH_4	
M1	1	0.94 ± 0.50	0.164 ± 0.07	5.7 ± 0.42
M2	3	1.93 ± 0.10	0.324 ± 0.02	6.0 ± 0.36
M3	10	2.87 ± 0.15	0.258 ± 0.02	11.1 ± 0.46
M4	20	2.13 ± 0.21	0.246 ± 0.01	8.7 ± 0.38
M5[a]	10	4.02 ± 0.22	0.356 ± 0.02	11.3 ± 0.31

[a] M5 was prepared with double amount of silicon in the gel.

increased linearly as a function of the logarithm of seed ARs from $(0.941 \pm 0.5) \times 10^{-7}$ to $(1.93 \pm 0.1) \times 10^{-7}$, and then to $(2.87 \pm 0.15) \times 10^{-7}$ mol m^{-2} s^{-1} Pa^{-1} for membranes M1, M2, and M3, respectively. N_2/CH_4 selectivity slightly increased from 5.7 ± 0.42 to 6.0 ± 0.36 when increasing the AR of seeds from 1 to 3. The maximum N_2/CH_4 selectivity, 11.1 ± 0.46, was obtained for membrane M3 by further increasing AR to 10. Separation performance of M4 was similar to that for M2. As discussed earlier, the degraded separation performance can be ascribed to a thicker effective membrane thickness. Therefore, the N_2 permeance and selectivity over CH_4 are expected to increase when an appropriate support is used.

N_2/CH_4 mixture separations at elevated temperatures (40, 55, and 70 °C) were also performed for SAPO-34 membranes (Figure 3a and Figure S6). For M3, both N_2 and CH_4 permeances increased with the increase of temperature, but N_2 permeance increased more slowly than that of CH_4, resulting in slightly decreased N_2/CH_4 selectivity. The highest N_2 permeance for this membrane was $(3.23 \pm 0.32) \times 10^{-7}$ mol m^{-2} s^{-1} Pa^{-1} at 70 °C, and the highest N_2/CH_4 separation selectivity was 11.1 ± 0.46 at 22 °C. Importantly, we also observed a substantial increase in N_2 permeance without sacrificing N_2/CH_4 selectivity for membranes prepared with doubled silicon content in the gel. For example, M5 with higher Si/(Si + Al + P) ratio (Table S2) showed the highest N_2 permeance of $(4.93 \pm 0.25) \times 10^{-7}$ mol m^{-2} s^{-1} Pa^{-1}) at 70 °C and N_2/CH_4 selectivity of 11.3 ± 0.31 at 22 °C (Figure 3a, empty symbols). SEM results confirmed that M5 was well intergrown and had a similar thin thickness of 2 μm as M3 (Figure S7 and Figure S4c,d). Increased N_2 permeance may result from the different framework compositions that may slightly change the crystal structure and thus affect diffusion in SAPO-34 crystals.[9b,14] To prove this assumption, we selected a tight-fit molecule to SAPO-34 pores, propane, and used its adsorption uptake kinetics to explore the small potential change of the SAPO-34 structure upon compositional change. Propane adsorbs slowly on SAPO-34 crystals, allowing us to precisely monitor its diffusivity change that may tell us slight structure variation upon framework compositional change. SAPO-34 crystals with different compositions were collected from the gels used for M3 and M5 synthesis and denoted as crystal-3 and crystal-5, respectively. Adsorption kinetics profiles (M_t/M_∞ vs. time) were shown in Figure 3b. SAPO-34 with higher Si content (crystal-5) showed a larger slope which corresponds to a faster diffusion of propane in SAPO-34 pores (Supporting Information). This indicates incorporating more Si into the structure slightly increases the SAPO pore size. Therefore, fine-tuning of the framework composition may influence diffusion of molecules in SAPO-34 crystals and thus may be a viable way of further improving the membrane separation performance if the membrane quality is high and thus the flux contribution from defects negligible.

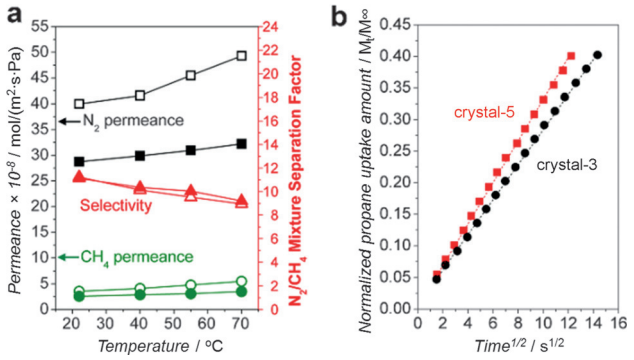

Figure 3. a) Equimolar N_2/CH_4 mixture separation at different temperatures by M3 (solid symbols) and M5 (open symbols). The pressure drop was 175 kPa with a permeate side pressure at 101 kPa. b) Propane adsorption kinetics at 22 °C on crystal-3 and crystal-5 collected in M3 and M5 preparation, respectively. M_t is the adsorbed amount of propane at time t, and M_∞ is adsorbed amount of propane at equilibrium.

Figure 4 compared our SAPO-34 membranes to other reported inorganic membranes[3,9e,15] and polymer membranes presented in the "Robeson" plot[4] for the N_2/CH_4 separation. The SEM thicknesses were used in the calculation of N_2 permeabilities (permeance × membrane thickness) for our SAPO-34 membranes. SAPO-34 membranes from this work were significantly above the upper bound and also showed superior performance to other inorganic membranes. Moreover, our membranes were highly reproducible using the reported synthetic and secondary growth technologies. We also found that the SAPO-34 membranes demanded a sufficient drying period to achieve and reproduce their high permeance and selectivity because of the moisture sensitivity of the SAPO-34 structure. To apply our approach for fabrication of commercially available membrane tubes, uniformity of the seeding layer prepared by rubbing might be a key challenge. The mitigation strategy is to use a more scalable dip-coating technique instead of rubbing; a previous study has shown that both rubbing and dip-coating seeding methods had yielded SAPO-34 membranes with similar CO_2/CH_4 separation properties and membrane performances were slightly more reproducible when dip-coating was used.[16]

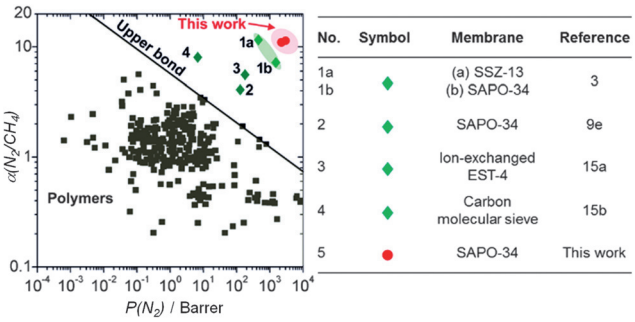

Figure 4. Comparison of polymer membranes presented in the Robeson plot and other inorganic membranes for N_2/CH_4 separation.

In summary, by using high-aspect-ratio SAPO-34 seeds, we grew thinner SAPO-34 membranes of higher quality and achieved simultaneous increase of N_2 permeance and N_2/CH_4 mixture selectivity. Also, by incorporating more Si into the crystal structure the N_2 permeance significantly increased,

while maintaining the N_2/CH_4 selectivity. This may result from the slight variation in the crystal structure upon compositional change. The best membranes showed a N_2 permeance as high as $(4.93 \pm 0.25) \times 10^{-7}$ mol m^{-2} s^{-1} Pa^{-1} at 70 °C and a N_2/CH_4 selectivity of 11.3 ± 0.31 at 22 °C for a 50/50 N_2/CH_4 mixture. Their separation performance is superior to those of state-of-the-art membranes. We expect that the high-aspect-ratio seeds may also be used for growth of high-quality, thickness-reduced zeolite membranes with other crystal structures which could be applied for different mixture separations.

Acknowledgements

We thank the financial support by Advanced Research Projects Agency-Energy (ARPA-E), U.S. Department of Energy, under award number DE-AR0000247.

Keywords: crystal seeds · inorganic chemistry · materials science · membranes · separation

How to cite: *Angew. Chem. Int. Ed.* **2015**, *54*, 10843–10847
Angew. Chem. **2015**, *127*, 10993–10997

[1] R. W. Baker, K. Lokhandwala, *Ind. Eng. Chem. Res.* **2008**, *47*, 2109.
[2] S. G. Li, Z. W. Zong, S. J. Zhou, Y. Huang, Z. N. Song, X. F. Feng, R. F. Zhou, H. S. Meyer, M. Yu, M. A. Carreon, *J. Membr. Sci.* **2015**, DOI: 10.1016/j.memsci.2015.03.078.
[3] T. Wu, M. C. Diaz, Y. Zheng, R. Zhou, H. H. Funke, J. L. Falconer, R. D. Noble, *J. Membr. Sci.* **2015**, *473*, 201.
[4] L. M. Robeson, *J. Membr. Sci.* **2008**, *320*, 390.
[5] a) M. P. Bernal, J. Coronas, M. Menendez, J. Santamaria, *AICHE J.* **2004**, *50*, 127; b) J. C. Poshusta, R. D. Noble, J. L. Falconer, *J. Membr. Sci.* **1999**, *160*, 115; c) M. A. Snyder, M. Tsapatsis, *Angew. Chem. Int. Ed.* **2007**, *46*, 7560; *Angew. Chem.* **2007**, *119*, 7704.
[6] a) X. H. Gu, J. H. Dong, T. M. Nenoff, *Ind. Eng. Chem. Res.* **2005**, *44*, 937; b) J. C. White, P. K. Dutta, K. Shqau, H. Verweij, *Langmuir* **2010**, *26*, 10287.
[7] Y. Cui, H. Kita, K. Okamoto, *J. Mater. Chem.* **2004**, *14*, 924.
[8] a) T. Tomita, K. Nakayama, H. Sakai, *Microporous Mesoporous Mater.* **2004**, *68*, 71; b) S. Himeno, T. Tomita, K. Suzuki, K. Nakayama, K. Yajima, S. Yoshida, *Ind. Eng. Chem. Res.* **2007**, *46*, 6989.
[9] a) M. A. Carreon, S. Li, J. L. Falconer, R. D. Noble, *Adv. Mater.* **2008**, *20*, 729; b) S. Li, J. L. Falconer, R. D. Noble, *Adv. Mater.* **2006**, *18*, 2601; c) M. A. Carreon, S. Li, J. L. Falconer, R. D. Noble, *J. Am. Chem. Soc.* **2008**, *130*, 5412; d) R. Zhou, E. W. Ping, H. H. Funke, J. L. Falconer, R. D. Noble, *J. Membr. Sci.* **2013**, *444*, 384; e) S. Li, J. L. Falconer, R. D. Noble, R. Krishna, *J. Phys. Chem. C* **2007**, *111*, 5075.
[10] K. Varoon, X. Zhang, B. Elyassi, D. D. Brewer, M. Gettel, S. Kumar, J. A. Lee, S. Maheshwari, A. Mittal, C.-Y. Sung, M. Cococcioni, L. F. Francis, A. V. McCormick, K. A. Mkhoyan, M. Tsapatsis, *Science* **2011**, *334*, 72.
[11] M. Tsapatsis, *AICHE J.* **2014**, *60*, 2374.
[12] a) B. Han, C. H. Shin, P. A. Cox, S. B. Hong, *J. Phys. Chem. B* **2006**, *110*, 8188; b) N. Najafi, S. Askari, R. Halladj, *Powder Technol.* **2014**, *254*, 324.
[13] Structural information of CHA-type zeolites can be found in the Database of Zeolite Structures at http://www.iza-structure.org/databases/.
[14] S. Li, J. L. Falconer, R. D. Noble, *Microporous Mesoporous Mater.* **2008**, *110*, 310.
[15] a) G. Q. Guan, K. Kusakabe, S. Morooka, *Microporous Mesoporous Mater.* **2001**, *50*, 109; b) X. Ning, W. J. Koyos, *Carbon* **2014**, *66*, 511.
[16] E. W. Ping, R. F. Zhou, H. H. Funke, J. L. Falconer, R. D. Noble, *J. Membr. Sci.* **2012**, *415–416*, 770.

Received: April 24, 2015
Revised: July 7, 2015
Published online: August 6, 2015

